Source mechanisms of Vulcanian eruptions at Mt. Asama, Japan, inferred from volcano seismic signals

Earthquake Research Institute

Takao Ohminato

Submitted to GSL

11 February, 2007

Revised on 24 December, 2007

Abstract

During the 2004 Asama volcanic activity, five summit eruptions, accompanied by the broadband seismic signals were observed. We re-analyze the broadband waveform data analyzed by Ohminato *et al*. (2006) using relaxed restrictions. The results are essentially the same as those shown in the previous study.

The results of the waveform inversions that assume a point source show that the force system is dominated by vertical single force components. The source depths with dominant single force components are 200-300 m beneath the summit crater. In the source-time history of the vertical single-force component, two downward forces separated by an upward force lasting for 5-6 s, are clearly seen.

We conduct a grid search for the best combination of two point sources, each consisting of a single-force component. The best waveform-match solution was obtained when one of them is positioned near the top of the conduit, and the other source is positioned 2000 m below the upper source.

When a combination of a single-force and a moment-tensor components is assumed for the two point-source model, the moment source is located out of the vertical hypocenter distribution, suggesting steeply inclined conduit.

Keywords: Mt. Asama, vulcanian eruption, very-long-period signals, single-force

After a quiescent period lasting 21 years, Mt. Asama erupted on 1 September, 2004. This initial explosion was followed by four eruptions. Mt. Asama is now relatively quiet in terms of volcanic activity. Ohminato *et al*. (2006) analyzed very-long-period (VLP) seismic waveforms accompanying these eruptions, and showed that the corresponding force systems are all dominated by a vertical single-force component. However, these authors restricted their waveform analyses to point sources located along a vertical line extending below the center of the summit crater. They also limited their investigation to two point sources. One of the two point sources had a mechanism consisting of single-force components, and the other had a mechanism consisting of moment-tensor components.

In this paper, we re-analyze the same data as Ohminato *et al*. (2006). We conduct a grid search for the source location not only in the vertical direction but also in the horizontal direction. A more extensive combination of source mechanisms, such as a combination of two point sources with mechanisms consisting of single-force components, is also tested. The dates and times used throughout this paper are Japan Standard Time.

Setting of Asama Volcano

Mt. Asama, located in central Japan, is one of the most active andesitic volcanoes in Japan (Figure 1). The summit elevation is 2560 m above sea level, and the active summit crater is 450 m in diameter and 150 m in depth. To the west of Mt. Asama is a row of older Quaternary volcanoes collectively known as Eboshi Volcano. The

volcanism near Mt. Asama appears to have progressed eastward, with Asama volcano representing the eastern end and youngest member of the row.

The first eruption recorded in historic documents occurred in 685 AD. After a 400-year period of apparent dormancy, a large-scale Plinian eruption in 1108 produced more than 1 km^3 of volcanic ejecta. In 1783, another Plinian eruption wiped out 4 villages and killed several hundred people (Aramaki 1963). Most of the eruptions since then have been of the vulcanian type. In the early 1900s, vulcanian and sub-plinian eruptions were frequently observed. From 1960 to 2004, Mt. Asama was relatively calm except for 1973 and 1984. The last major eruptions were vulcanian and occurred during the periods 1973-1974 and 1982-1983.

Volcanic activity in 2004

GPS observations indicated magma injection beneath Mt. Asama from the middle of July through the end of August 2004 (Aoki *et al*. 2005, Takeo *et al*. 2006). The source of the ground deformation inferred from the GPS data was modeled as the opening of a nearly vertical dyke at 2-3 km beneath the Eboshi-Asama volcanic row, west of the summit of Mt. Asama. From late 1999, the seismic activity started demonstrating a clear upward trend, and the eruption in 2004 occurred in the middle of this increasing trend. Starting in 2002, VLP seismic signals (~10s) with unique waveforms were frequently observed and maximum temperatures at the bottom of the crater in excess of 200°C were recorded (Takeo *et al*. 2006).

An intense seismic swarm started at about 3 pm on 31 August, 2004 (Nakada *et al*. 2004), and the first vulcanian eruption occurred at 20:02 on 1 September. From 15 to 17

September, Mt. Asama continuously emitted volcanic ash that reached as far as metropolitan Tokyo about 130 km away. Following this ash emission stage, four more eruptions occurred on 23, 29 September, 10 October, and 14 November. The estimated amounts of ash deposits are 4.9×10^7 kg, 8.5×10^6 kg, 1.3×10^7 kg, 2.8×10^6 kg, and 2.5×10^7 kg, for eruptions on 1, 23, 25, and 29 September, 10 October, and 14 November, respectively (Yoshimoto *et al*. 2005). The explosion on 1 September was the largest in terms of the amounts of ash deposits, while the explosion earthquake on 23 September was the largest of the five explosion earthquakes that occurred during the 2004 activity (Ohminato *et al*. 2006).

GPS observations indicate that the propagation of the dyke beneath the Eboshi-Asama volcanic row, which started in mid July, continued during the volcanic activity (Aoki *et al*. 2005, Murakami *et al.* 2005). The VLP seismic activity with unique waveforms disappeared a few days before the eruption on 1 September, suggesting a change in the volcanic edifice as a precursor to the eruptions that followed (Yamamoto *et al*. 2005).

The hypocenter distributions before, during and after the volcanic activity in 2004, fall into two groups (Takeo *et al*. 2006). One group consists of a vertical distribution of sources ranging from the bottom of the summit crater to a depth of 1 km below sea level, outlining the vertical extension of the volcanic conduit. The other group includes a horizontal distribution of sources extending 2 km in the west-northwest direction from the bottom of the vertical distribution of the sources. The latter hypocenter distribution coincides with the top edge of the vertical dyke inferred from GPS observations.

Seismic network around Mt. Asama

The seismic network in operation before the eruption on 1 September consisted of short-period seismic sensors with narrow dynamic range data loggers and one broadband seismic sensor (STS-2) positioned 4 km from the summit. Owing to the narrow dynamic range of these sensors and also due to the extremely large amplitude of the accompanying air shock, many of the seismic records from this eruption are saturated and only five stations are available for analysis.

We installed temporary broadband stations featuring 7 broadband sensors around Mt. Asama after the ash-emission activity on 15 - 17 September (Figure 1). Three stations were equipped with STS-2 sensors with a natural period of 120 s, and four stations were equipped with CMG-3T sensors with natural periods ranging from 100 to 360 s. The second eruption occurred on 23 September, one week after the installation of the temporary network. Eventually, we recorded four of the five eruptions that occurred during the activity of 2004 with 8 broadband seismic stations. We checked the broadband sensor responses and sensor orientations using teleseismic signals dominated by 20 s surface waves. We also checked the sensor orientations using a gyro-compass with 1° accuracy. In Figure 2, waveforms of 5 eruptions recorded at FJM and MAE are shown. Since the broadband station MAE was not in operation when the event on 1 September occurred, we show the waveforms recorded at FJM, the second closest station to the summit, instead of the waveforms recorded at MAE.

Data analyses

In the following, we will focus on the results of analyses for the event on 23 September as this event had the largest amplitude among the 5 eruptions. For this event, which occurred on 23 September, the broadband seismic records from 8 stations were available.

Our search for source location and source mechanism uses the inversion method of Ohminato *et al*. (1998). This method is based on a very simple and straightforward idea. Assuming a point source, the observed waveforms are expressed by the linear combination of Green's functions convolved with the appropriate source-time functions for three single-force components and six moment-tensor components. The combination of the source-time functions that best explains the observed waveforms is then determined by solving a set of linear equations. Our search for the best-fitting signal is carried out for trial point sources distributed in a uniform mesh sampling the inferred source volume. The source volume is defined around the initial source location based on the results of particle motion analyses. For details of the procedure, see Ohminato *et al*. (1998).

The Green's functions used in our waveform analyses are calculated by the 3-dimensional finite-difference method (Ohminato & Chouet 1997) assuming a homogeneous medium with realistic topography. The P- and S-wave velocities and density values used in our calculations are 3280 m/s, 1660 m/s, and 2400 kg/m^3, respectively. These velocity values are determined so that the observed travel time residuals are minimized (Ohminato 2006). The density value is based on the gravity survey around Mt. Asama (Onizawa *et al*. 1996).

The onsets of the particle motions for the eruption on 23 September point to the summit crater. As stated above, earthquake hypocenters are distributed vertically from

the bottom of the crater to 1 km below sea level. Considering the results of particle motion analyses together with the hypocenter distribution, we consider a source volume of 1.6 km in width in both the north-south and east-west directions, and 3.2 km in the vertical directions. This volume includes almost the entire vertical hypocenter distribution beneath the summit. In the uniform mesh sampling the volume, the grid size of 50 m is used, and thus the number of grid points searched for is approximately 70000.

Possible source models expressed by the moment tensors and single forces

Here, we briefly summarize several source-models relevant to volcanic processes so that the concepts being used in this paper can be understood easily. The following explanation follows mainly Chouet (1996).

The solutions obtained from waveform analyses yield information about the force system exerted in the source region. The derived force system does not image the real forces but represents an equivalent system of force (Aki & Richards 1980). We must then interpret the physical meaning of these equivalent forces.

Figure 3 shows some of the force systems that represent seismic sources in volcanoes. For example, a tension crack opening or closure is represented by 1:1:3 amplitude ratios among the three diagonal components of the diagonalized moment tensor. If the ratio is 2:2:1, it is interpreted as a radial oscillation of a cylinder. If the ratio is 1:1:1, it is an isotropic volume change. For these ratios, $\lambda = \mu$ is assumed, where λ and μ are the Lamé coefficients of the rock matrix. For rock near liquidus temperature, $\lambda = 2\mu$ may be more appropriate, yielding the ratios 1:1:2 and 3:3:2 for oscillations of crack and cylinder, respectively. These three examples represent the volume change at the source

(Figure 3(a)). The two examples shown in Figure 3(b) correspond to physical processes that produce no net volume change and are called "Compensated Linear Vector Dipole" or CLVD.

Some force systems are not necessarily expressed by the moment-tensor components. Single-force components are also observed in nature. One well-studied example of single-force component in nature is the model introduced by Kanamori *et al*. (1984) to quantify the explosive eruption at Mt. St. Helens in 1980. In this model, a pressurized portion of the volcanic conduit capped by a lid is assumed. When the lid is removed suddenly, a vertical single force and an isotropic implosive source are generated (Figure 3(c)). The drag force due to viscous flow through a narrow channel is another possible mechanism for a single force (Figure 3(d)).

As proposed by Takei and Kumazawa (1994), a single force can be generated by an exchange of linear momentum between the source region and the rest of the earth. Suppose a block of rock is attached to the ceiling of a magma chamber. When the block detaches from the ceiling, it starts falling through the magma chamber with increasing velocity. The block gradually looses the downward velocity as it approaches the bottom of the chamber. Finally, the block reaches the bottom of the chamber. During this process, there is a downward acceleration of the center of mass of the source volume, followed by a downward deceleration of the center of mass of the source volume. The resulting reaction force in the surrounding medium is an upward force followed by a downward force (Figure 3(e)).

Note again that what we obtain from seismic waveform analyses is a force system relevant to volcanic processes but not the physical process itself.

Results of the waveform analyses for cases assuming a point source

Ohminato *et al*. (2006) assumed that the source locations are beneath the center of the summit crater, and they searched in the vertical direction guided solely by particle motion analyses. In this study, in contrast to the previous study, we search for source locations in a volume that include most of the hypocenter distribution of the volcanic earthquakes as stated above. As a first step, we test seven equivalent force cases assuming a single point source (Table 1). The waveform matches for the vertical components at MAE, the closest station, are shown in Figure 4. The source locations for the seven cases have slight offsets in the horizontal direction. The offsets are 200-300 m southwest (Case 1, Case 4, Case 5, Case 6, and Case 7) or southeast (Case 2 and Case 3) of the center of the summit crater, and thus the source locations obtained in this study are close to that obtained by Ohminato *et al*. (2006). The errors are smaller than that obtained in the previous study because of the relaxed condition for the horizontal source location.

In order to evaluate the trade-off between the data fit and the number of free parameters, we use Akaike's Information Criterion (AIC) (Akaike 1974) that is defined as AIC = $N_s \ln(e) + 2N_m$ in which the constant term is omitted. N_s is the number of data fitted by the model, and is calculated by the number of data traces multiplied by the number of samples in each trace. e represents the squared error. N_m is the number of free parameters, and is calculated by the number of assumed single-force and moment-tensor components multiplied by the number of samples of each source-time history. The preferred model is the one with the lowest AIC value. To have a lower AIC is better than to have a lower residual.

The AIC values obtained in this study (Table 1) are larger than that obtained in the previous study (Ohminato *et al*. 2006, Table 2) because the number of samples in each seismic trace and the number of elementary source pulses used to represent the source time function are 150 and 75, and are half of those used in the previous study. Details of the results of the seven cases are as follows.

Case 1: The source mechanism includes a vertical single-force component only (abbreviated as 'Fz'). In this simplest case, the vertical components of the waveforms are well explained, but the horizontal components are poorly explained and thus the residual error is large. The source location is 200 m west and 50 m south of the center of the summit crater. The source elevation is 2450 m above sea level. Hereafter, we use the Cartesian coordinate with origin set at sea level beneath the center of the summit crater to indicate source locations. The source location for Case 1 is expressed as (-200, -50, 2450).

Case 2: The source mechanism consists of six moment-tensor components and no single force (abbreviated as '6Mom'). Although the number of free parameters is six times larger than that for Case 1, the AIC value for this case is smaller than that for Case 1 owing to an improved waveform match, especially in the horizontal components. Note, however, that the waveform match in the vertical components is degraded compared to Case 1. The source location for Case 2 is (200, -200, 2100).

Case 3: The source mechanism consists of six moment-tensor components and two horizontal single-force components (abbreviated as '6Mom+2SF'). Additional horizontal single-force components improves both error and AIC. In this case, however, the vertical components of the waveforms are not well explained as in Case 2. The source location for Case 3 is (200, -300, 2100).

Case 4: The source mechanism consists of three single-force components (abbreviated as '3SF'). Although the error reduction is worse than that for Case 3, a smaller AIC value is obtained owing to the smaller number of free parameters compared to Case 3, and thus Case 4 is better than Case 3 in terms of AIC. In this case, the vertical components of the waveforms are well explained. The source location for this case is (-200, -100, 2250).

Case 5: The assumed source mechanism consists of six moment-tensor components and one vertical single-force component (abbreviated as '6Mom+Fz'). Comparison between this case and Case 2 clearly shows that the addition of the vertical single-force component dramatically improves the waveform match, and thus results in a smaller AIC value. This observation supports the idea that the 'Fz' is an indispensable component for the mechanism of the eruptions at Mt. Asama. The source location for Case 5 is (-200, -100, 2150).

The results of the above five cases clearly show that the 'Fz' component is indispensable for explaining the vertical components of the observed waveforms. The question arises, then, of which components are important for explaining the horizontal component of the waveforms. In order to clarify this, we test additional cases.

Case 6: In this case, the source mechanism consists of an isotropic component and three single-force components (abbreviated as 'ISO+3SF'). We replace the 6 moment-tensor component in Case 5 with an isotropic component, and we add two horizontal single-force components. These changes reduce the AIC slightly. The effect of the reduction of the number of free parameters overcomes the small increase in the residual error compared to Case 5. For both Cases 5 and 6, the vertical components of the waveforms are already well explained by the 'Fz' component that is included in both

cases. Thus, a comparison between Case 5 and Case 6 suggests that the contribution of the non-isotropic (deviatoric) components of the moment tensor and the contribution of the two-horizontal single-force components to the horizontal components of the waveforms are almost the same. In other words, the horizontal components of the observed waveforms are explained similarly by both a deviatoric component of the moment-tensor or two horizontal single-force components. The source location for Case 6 is (-250, -150, 2200).

Case 7: Finally, we tested the source mechanism composed of six moment-tensor components and three single-force components (abbreviated as '6Mom+3SF'). This case resulted in the best error residual and best AIC solution. A comparison among Case 5, Case 6 and Case 7 indicates that both the deviatoric components of moment tensor and the two horizontal single-force components are indispensable for explaining the observed waveforms, and they cannot compensate for each other's contributions. The source location for Case 7 is (-100, -100, 2200).

Figure 5 shows the distribution of the residual error in the volume where the grid search for the best source location was conducted. The two horizontal axes in the north-south and east-west directions represent distances from the center of the summit crater. The vertical axis shows the elevation above sea level. In this figure, six horizontal slices are shown. The residual value increases from blue to red. The colour scale on the right is from 100 % to 160 % of the smallest residual. The distribution corresponding to Case 7 is shown. The residual distribution is simple and has only one global minimum. Similar simple residual distributions are obtained for all seven cases stated above. One-point-source solutions are stable and robust.

Results of the waveform analyses for cases assuming separated sources

In Ohminato *et al*. (2006), it was assumed that the explosion source was composed of two point sources; one of them corresponded to three single-force components, and the other corresponded to six moment-tensor components. They fixed the horizontal source location at the center of the summit crater and searched for the best combination of depths for these two sources in the vertical direction. For the best AIC solution, the depth of the single-force source was at the bottom of the crater, and the depth of the six moment-tensor source was at 400 m beneath the single-force source. The source mechanism of the moment-tensor component was found to be an almost isotropic volume change.

For the next step in our study, we investigate sources consisting of two point sources. In this investigation, one of the two sources has a fixed location and a search for the other source location is made grid by grid. We search not only in the vertical direction but also in the horizontal directions. As discussed above, the results of Cases 1 through 4 show that a source composed of three single-force components is indispensable. The source locations for Cases 4 through 7, all including 'Fz' component, are almost the same. Accordingly, we fix the source location of the single-force component at the location (-200, -100, 2250) that is obtained for Case 4, and search for the location of another point source. We test three cases for the two-point-source model. We assume 'ISO', '3SF', and '6Mom' for the source mechanisms of the second point source, whose location is grid-searched. They are abbreviated as '3SF + ISO', '3SF + 3SF', and '3SF + 6Mom', and are referred to as Case 8, Case 9, and Case 10, respectively. Errors and the AIC value for Cases 8, 9, and 10 are shown in Table 2.

The global minimum for Case 8 is obtained for an isotropic source located 1 km east-southeast of the summit crater. This location is beneath station MAE, which is the station closest to the summit. Near this station, there is nothing that suggests shallow hydrothermal or magmatic activity such as fumaroles, vents, or cracks on the ground surface. Judging from the distance from the summit crater and the surface condition around MAE station, this location is highly inappropriate as a source of the explosion signal. We find a second local minimum at (-250, -150, 2200). This position is the same as the source location obtained for Case 6. We therefore discard the former position and adopt the latter.

Although we assumed separate sources composed of '3SF' and 'ISO' in this case, the source location of the 'ISO' component found to be very close to the location of the fixed point source of '3SF'. The separated source of '3SF + ISO' can be regarded as a point source. The residual for this solution is much smaller than that of the solution composed of '3SF' and 'ISO' obtained at (0, 0, 2200) by Ohminato *et al*. (2006). It is highly likely that the source locations obtained by these authors were inaccurate positions resulting from their imposed restriction of horizontal source locations fixed beneath the center of the summit crater.

In Case 9, we again observe that a minimum residual error is obtained nearly 1 km east of the summit crater. Such a solution is unrealistic for the same reason stated for Case 8, and so we discard it. We find a second-best local minima beneath the summit at two distinct elevations, namely at (-400, -100, 1500) and (-300, -100, 0) (Figure 6). The former is 1500 m above sea level and the latter is at sea level. The latter solution gives us a slightly better AIC value, although the difference in AIC is very small. In Table 2,

the result for the latter is shown. The source time functions corresponding to the deep '3SF' source at sea level and to the fixed '3SF' source are illustrated in Figure 7.

In Case 10, one point source of '3SF' is fixed at the location for Case 4 and the other point source of '6Mom' is grid-searched. The best source location for a source of '6Mom' is (450, -200, 1250). The global minimum is obtained at the southeast of the summit crater, and the location is out of the vertical hypocenter distribution. For other two cases, Case 8 and Case 9, the locations of the 'unfixed' components, 'ISO' and '3SF', are within the hypocenter distribution, showing that the locations for Cases 8 and 9 are not attracted to MAE station.

Discussion

Characteristic source-time history of 'Fz'

The solution obtained for the 23 September event assuming a point source is essentially the same as that obtained by Ohminato *et al*. (2006). The source-time history of the vertical single-force component 'Fz' is characteristic. Figure 8 shows the source-time histories of 'Fz' for all five events. These are vertically aligned so that their first downward phases coincide with each other. We can summarize the characteristics seen in the source time function of 'Fz' as follows.

For all the source-time histories of 'Fz', (i) the initial motion of the vertical force is always downward; (ii) it is followed by an upward force; (iii) there is another downward force 5-6 sec after the first downward force.

The above-mentioned characteristic source-time histories of 'Fz' are interpreted by Ohminato *et al*. (2006) as follows.

(1) Before an eruption, the source region is pressurized. This region is located at the top of the conduit. (2) A lid at the top of the pressurized conduit is suddenly removed and downward and implosive forces are excited. This corresponds to the source process proposed by Kanamori *et al*. (1984) as explained earlier in Figure 3(c). (3) The depressurized magma increases its volume due to vesiculation and starts ascending in the conduit. The highly viscous andesitic magma exerts an upward force on the conduit wall. This is the source process schematically shown in Figure 3(d). During this stage, the observed vertical single force is expressed by the superposition of two vertical forces. One is the downward force that is gradually increasing after the sudden removal of the lid as expected from the Kanamori's model. The other is the upward force originated from the viscous ascending magma. Since the observed vertical force is upward during this stage, the amplitude of the upward force is larger than the downward force. (4) Finally, explosive fragmentation starts when the magma reaches some critical depth. (5) Magma viscosity disappears due to magma fragmentation, and thus the upward viscous force also disappears. Since the vertical force component is the superposition of two force components, the sudden disappearance of the upward viscous force results in the appearance of the second downward force.

Conservation of total linear momentum

Ohminato *et al*. (2006) attributed the origin of the upward single force to the viscous drag force exerted on the wall of the volcanic conduit by the ascending viscous magma.

The way linear momentum is exchanged between the ascending magma column and the rest of the earth is slightly complicated and requires some explanation.

Magma ascends in the conduit because it gains upward linear momentum from the rest of the earth. In return, the rest of the earth receives downward linear momentum. The exchange of the linear momentum mainly takes place at a certain depth in the conduit. A part of the upward linear momentum that the ascending magma column receives from the rest of the earth is returned to the earth through the viscous drag force exerted on the shallow portion of the conduit. The total linear momentum that the rest of the earth receives from the ascending magma column consists of the momentum transferred at certain depths and momentum transferred through the upward viscous drag force exerted near the top of the conduit.

The shallow force should be observed as an upward force. Naturally, if the viscosity of the magma is low enough, the shallow force is not detectable. In contrast, the excitation of the seismic signals of observable amplitude by the force corresponding to the exchange of linear momentum at the deep portion in the conduit depends on the depth where the momentum exchange takes place. Note that the upward linear momentum of the magma column must balance the downward linear momentum gained by the rest of the earth. The force exerted on the shallow portion of the conduit and the force exerted at deep portion of the conduit do not necessarily balance. The deep force must be stronger than the shallow force for the magma column to gain upward linear momentum. What matters here is the depth of the zones where the single forces are applied.

The upward force may act mainly on a relatively short segment of conduit near the top of the magma column, where the pressure gradient is the largest (e.g. Sparks 1997),

and thus the traction force on the conduit wall is the largest. In contrast, the portion of the conduit where the downward force is exerted probably extends over a significant depth range. It is difficult to specify the extent of the portion of the magma column that exerts the downward force on the conduit wall. Such a portion of the magma column can be extended from the vesiculation depth of 2-3km to the greater depth of few kilometers down to the magma chamber. The contribution of the portion of conduit, which receives the downward force from the magma column, to the excitation of seismic signals may not be well observed because of the large hypocentral distance to the seismic stations (Figure 9(a)).

There may be another shape for the distribution of downward single force over the conduit wall. Suppose there is a discontinuity in the conduit at a certain depth. This discontinuity may be a constriction or a sharp bend in the conduit. In this case, the downward force necessary to conserve the linear momentum would concentrate at the discontinuity, and the distribution of the vertical single force in the conduit may be as shown in Figure 9(b). In this case, the portion where the downward force is exerted is much shallower than in the case where there is no discontinuity, and the seismic signals associated with the downward force can be observed.

In the rest of this section, we investigate whether a source composed of two point sources, each with '3SF', can explain the observed waveform better than a single point source. If a source consisting of one point source composed of '3SF' explains the observed waveform better than a source consisting of two point sources, then the force distribution shown in Figure 9(a) is preferable. In contrast, if a second point source composed of '3SF' is discovered at a depth that is not extremely great, then the model of Figure 9(b) would be better.

A model of one or two point sources may seem to be too simple as the actual source must be a fully continuous extended source. This simplistic model consisting of a few point sources represents an intermediate step from the traditional single point source model to the extended source model. A fully extended source is beyond the scope of this study, however.

In Case 9, two source locations are obtained. The source location of the shallower source at 1500 m is in the middle of the vertical hypocenter distribution beneath the summit crater, and the source location of the deeper source at sea level coincides with the depth where the hypocenter distribution changes its spatial density significantly (Figure 10). The sudden change in density of the hypocenter distribution at sea level suggests the existence of a certain change in the physical condition around the conduit at this depth. If there is a certain condition change in the conduit at sea level, then the observation that the deep '3SF' source is slightly better than the shallow '3SF' source may suggest that the model with conduit constriction (Figure 9(b)) is preferable to the model with no constriction (Figure 9(a)).

To interpret the source-time functions of the six force components illustrated in Figure 7 is not easy. The horizontal components have the amplitudes almost equivalent to that of the vertical component. The behavior of the horizontal components of the shallow and deep sources looks as if they are compensating each other, and are mimicking the horizontal dipoles distributed along the vertical conduit. Similar behavior as the horizontal components is seen for the vertical components. On the source-time function similar to that of the one point-source case (see Figure 11, top), time functions of relatively high frequency are superimposed. These additional components at shallow and deep sources have opposite sign, and thus they are behaving as a vertical dipole.

These waveforms strongly suggest that in addition to the three single-force components, the six-moment-tensor components are necessary to explain the observed waveforms. Although the necessity of both single- force and moment-tensor components have been already suggested above, an inclusion of '6Mom' component in addition to two '3SF' will make the inversion unstable.

Location and interpretation of '6Mom' component

We summarize the source locations for the ten cases investigated in this study (Figure 10). The source locations for Cases 1 through 10 are compared with the hypocenter distribution of the volcanic earthquakes before, during, and after the 2004 Mt. Asama volcanic activity determined by Takeo *et al*. (2006) using the double-difference method (Waldhauser & Ellsworth 2000). For all of the cases that include the vertical single force component 'Fz', the source locations are within the vertical hypocenter distribution. In contrast to this, sources including '6Mom' components are liable to be located outside of the hypocenter distribution (an open circle for Cases 2 and 3, and a closed circle for Case 10). The results for Case 2, Case 3, and Case 7 indicate that the solution including the '6Mom' component and excluding vertical single force 'Fz' at the same time, are likely to be located east of the vertical hypocenter distribution of volcanic earthquakes. In contrast, other solutions including 'Fz', regardless of other source mechanisms included, are located within the hypocenter distribution. The point source solution for Case 7 includes both '6Mom' component and 'Fz' component, but the source location is inside of the vertical hypocenter distribution. This observation indicates that the

tendency that the '6Mom' source is attracted to the east is overwhelmed by the tendency that the 'Fz' source stays close to the vertical hypocenter distribution.

These observations suggest that the '6Mom' components are sensitive to waveform uncertainty, which can be attributed to unknown velocity and density structures. The reason that the solutions including the '6Mom' component are attracted to the closest station MAE may be that the amplitude of the waveforms observed at MAE is the largest due to the proximity of this receiver to the source, and thus the portion of the waveforms attributable to the uncertainty is also the largest. A source location near the station with the largest uncertainty is advantageous to reduce the overall waveform mismatch. Such a source can reduce the overall waveform mismatch only by explaining the waveform discrepancy of the waveforms at the largest amplitude station. This explanation would mainly work for the source of '6Mom,' which has the largest number of free parameters. For other sources, such as 'Fz', '3SF', and 'ISO' that have smaller numbers of free parameters, the explanation would not work effectively.

Figure 11 illustrates the source-time functions of the six components of the moment tensor and three components of single force for Case 7 and Case 10. The source-time functions for three single-force components are almost the same for these two cases, while the source-time functions for six moment-tensor components are significantly different for these two cases. This suggests that the six moment-tensor component does not necessarily reflect the physical process in the source region.

According to Kanamori's lid removal model, the amplitude of the moment-tensor component is obtained by the amplitude of the downward vertical single force multiplied by the extent of the pressurized portion of the conduit capped by a lid. Since the size of such a portion does not exceed the diameter of the summit crater of 400 m,

the amplitude of the moment-tensor component is at most 2×10^{13} Nm, which is much smaller than the amplitude of the moment-tensor components for both Cases 7 and 10. This estimation shows that the contribution of the volume change at the source related to the mass withdrawal from the system to the source-time functions for six moment-tensor component is small.

Furthermore, the source-time functions of three diagonal components for Case 10 are not necessarily in phase. This also makes it difficult to give a physical interpretation to the source-time functions of the moment-tensor component.

If we accept the fact that the solution displays a significantly lower residual error and clear minimum AIC compared to the other models, we need to interpret the source location in the east. Guided by the steeply dipping crack model obtained at Popocatépetl Volcano, Mexico (Chouet *et al*. 2005), it is conceivable that the upper conduit under Asama may be steeply inclined to the southeast and slightly offset from the distribution of earthquakes at a depth of 1.2 km below the summit crater. The fact that there is no hypocenter distribution that connects the summit crater and the '6Mom' source nor the hypocenter distribution connecting the '6Mom' source and the horizontal dyke inferred from GPS observations (shaded region in Figure 10) seems to be against the idea of steeply inclined conduit model. However, hypocenter distributions do not necessarily coincide with the magma path beneath volcanoes (e.g., Brancato & Gresto 2003), and thus, solely from the hypocenter distribution, we should not discard the inclined conduit model, which is favorable to the solution for Case 10.

Summary

We re-analyzed the waveform data associated with the vulcanian eruptions that occurred during the 2004 Mt. Asama activity. We loosened the restrictions on source locations and source mechanisms used in the previous study. The results are essentially the same as those obtained with more restrictions in the previous study. The source locations are slightly shifted in both the horizontal and vertical directions, but the characteristics of the source time histories of the vertical single force component do not change.

The source mechanisms include dominant vertical single force components. The source time history of the vertical single force starts with a large downward phase followed by an upward phase. After several seconds, another downward component appears. The initial downward force can be explained by the sudden removal of a lid capping the pressurized conduit. The following upward force can be interpreted as a drag force due to ascending viscous magma. The secondary downward force appears when the fragmented magma stops exerting an upward viscous drag force on the conduit wall, and the downward force due to the cap removal reappears.

The results of the analyses assuming two point sources suggest that the conduit has a constriction at sea level that works as a deep source of the secondary downward single force component. The results of the analyses assuming one point source of single-force components and another point source of six moment-tensor components suggest an inclined conduit model, although the inclined conduit is not necessarily suitable for the hypocenter distribution beneath the summit crater.

Acknowledgements

The author greatly thanks Steve Lane, who organized the wonderful WS and the Special Publication of the GSL on "Fluid motion in volcanic conduits: A source of seismic and acoustic signals". The author also thanks Jeff Johnson and Bernard Chouet, who gave us valuable and intense comments which improved the manuscript greatly. We also thank Jennie Gilbert, who patiently encouraged us to complete this work.

References

Akaike, H. A new look at the statistical model identification, IEEE Trans. Autom. Control, AC-9, 716-723, 1974.

Aki, K. and P. Richards, Quantitative Seismology Vol. I, 557 pp., Freeman, New York, 1980.

Aoki, Y., H. Watanabe, E. Koyama, J. Oikawa, and Y. Morita, Ground deformation associated with the 2004-2005 unrest of Asama Volcano, Japan, Bull. Volcanol. Soc. Japan, 50, 585-584, 2005 (in Japanese with English abstract).

Aramaki, S., Geology of Asama Volcano, J. Fac. Sci. Univ. Tokyo, 14, 229-443, 1963.

Brancato, A. and S. Gresta, High precision relocation of microearthquakes at Mt. Etna (1991-1993 eruption onset) : a tool for better understanding the volcano seismicity, J. Volcanol. Geotherm. Res., 124, 219-239, 2003.

Chouet, B., New methods and future trends in seismological volcano monitoring, in Monitoring and Mitigation of Volcano Hazards, edited by R. Scarpa and R. I. Tilling, pp.23-97, Springer-Verlag, Berlin, 1996.

Chouet, B., P. Dawson, and A. Archniega, Source mechanism of vulcanian degassing at Popocatepetl Volcano, Mexico, determined from waveform inversion of very long period signals, J. Geophys. Res., 110, doi:10.1029/2004JB003524, 2005.

Kanamori, H., J. Given, and T. Lay, Analysis of seismic body waves excited by the Mount St. Helens eruption of May 18, 1980, J. Geophys. Res., 89, 1856-1866, 1984.

Murakami, M., Magma Pluming system of the Asama volcano inferred from continuous measurement of GPS, Bull. Volcanol. Soc. Japan, 50, 347-361, 2005 (in Japanese with English abstract).

Nakada, S., M. Yoshimoto, E. Koyama, T. Tsuji, and T. Urabe, Comparative study of the 2004 eruption with old eruptions at Asama Volcano and activity evolution, Bull. Volcanol. Soc. Japan, 50, 303-313, 2005 (in Japanese with English abstract).

Ohminato, T. and B. Chouet, A free-surface boundary condition for including 3D topography in the finite difference method, Bull. Seismol., Soc. Am., 87, 494-515, 1997.

Ohminato, T., B. Chouet, P. Dawson, and S. Kedar, Waveform inversion of very-long-period impulsive signals associated with magmatic injection beneath Kilauea volcano, Hawaii, J. Geophys. Res., 103, 23839-23862, 1998.

Ohminato, T., M. Takeo, H. Kumagai, T. Yamashina, J. Oikawa, E. Koyama, H. Tsuji, and T. Urabe, Vulcanian eruptions with dominant single force components observed during the Asama 2004 volcanic activity in Japan, Earth Planets Space, 58, 583-593, 2006.

Onizawa, S., T. Matsushima, J. Oikawa, K. Okuda, M. Ichihara, K. Nawa, H. Gotoh, S. Udagawa, A. Takagi, T. Niina, H. Ohkunitani, N. Numata, S. Yoshida, M. Machida, S. Okubo, N. Gyoda, E. Koyama, H. Tsuji, M. D. Eleuterio, and M. Sawada, GPS and Gravity measurement at Asama volcano, Abst. Volcanol. Soc. Japan, 1996 Fall Meeting, B19, 1996 (in Japanese).

Sparks, R. S. J., Causes and consequences of pressurisation in lava dome eruptions, Earth Planet. Sci. Lett., 150, 177-189, 1997.

Takei, Y. and M. Kumazawa, Why have the single force and torque been excluded from seismic source models ?, Geophys. J. Int., 118, 20-30, 1994.

Takeo, M., Y. Aoki, and T. Ohminato, Magma supply path beneath Mt. Asama volcano, Japan, Geophys. Res., Lett., 33, doi:10.1029/2006GL026247, 2006

Waldhauser, F. and W. L. Ellsworth, A double difference earthquake location algorithm: method and application to the Northern Hayward Fault, California, Bull. Seis. Soc. Am., 90, 6, 1353-1368.

Yamamoto, M., M. Takeo, T. Ohminato, J. Oikawa, Y. Aoki, H. Ueda, S. Nakamura, H. Tsuji, E. Koyama, N. Osada, and T. Urabe, A unique earthquake activity preceding the eruption at Asama volcano in 2004, Bull. Volcanol. Soc. Japan, 50, 393-400, 2005 (in Japanese with English abstract).

Yoshimoto, M., T. Shimano, S. Nakada, E. Koyama, H. Tsuji, A. Iida, M. Kurokawa, Y. Okayama, M. Nonaka, T. Kaneko, H. Hoshizumi, Y. Ishizuka, R. Furukawa, K. Nogami, S. Onizawa, K. Niihori, T. Sugimoto, and M. Nagai, Mass estimation and characteristics of ejecta from the 2004 eruptions of Asama volcano, Bull. Volcanol. Soc. Japan, 50, 519-533, 2005 (in Japanese with English abstract)

Figure captions

Figure 1

Map of Mt. Asama and the seismic network. Eight closed circles are broadband stations. An open circle is a short period station, whose waveform records are shown in Figure 2. Contours represent 200 m elevation intervals. The inset shows the location of Mt. Asama in Japan.

Figure 2

Displacements recorded at FJM and MAE. Waveforms for the eruptions on 1, 23, 29 September, 10 October, and 14 November recorded at FJM and MAE are shown. Horizontal bars indicate time scales. Vertical bars indicate amplitude scale. For all the traces, sensor responses are corrected and the band-pass filter is applied in the 0.1-2 Hz band using a six-pole zero-phase Butterworth filter.

Figure 3

Examples of several source mechanisms expressed by moment tensor components and single force components in the context of the source of volcanic earthquakes. (a) Examples of source geometries including volume change. Crack, cylinder, and sphere are shown. The ratio under each panel represents the amplitude ratio of three eigenvalues of the corresponding moment tensor (reproduced from Chouet, 1996). (b) Examples of source geometries without volume change. These solutions are expressed by a combination of two volume sources with opposite signs. One of the volume sources corresponds to a volume expansion and the other corresponds to a shrinkage of

the same volume (reproduced from Chouet, 1996). (c) A model of vertical single force excitation proposed by Kanamori et al. (1984). A force system representing the sudden removal of a lid of a pressurized gas pocket near the ground surface is equivalent to a combination of a vertical single force and an implosive source. (d) A drag force due to viscous flow through a narrow path is a candidate for the source of the single force. (e) An example of source mechanisms with single force components proposed by Takei and Kumazawa (1994). An exchange of linear momentum between the source region and the surrounding rock is observed as the source of a vertical single force.

For all possible sources with single force components, the total linear momentum must be conserved.

Figure 4

Differences in waveform match for different source mechanisms corresponding to Cases 1 through 7. Waveforms are displacements and are band-passed at 0.1-2 Hz. A single point source is assumed in each case. The vertical component recorded at MAE during the event on 23 September is shown. Waveform matches around the initial downward phase for mechanisms including the 'Fz' component (Cases 1, 4-7) are good, while waveform matches for cases without 'Fz' (Cases 2 and 3) are significantly worse.

Figure 5

Residual distribution in the volume in which the grid search for the best source location is conducted. The horizontal axes show the distance from the center of the summit crater. The vertical axis shows elevation above sea level. Six horizontal slices with a vertical interval of 100 m are shown. The residual value increases from blue to red. The

bar range on the right is from 100% to 160 % of the smallest residual. Only the distribution corresponding to Case 7 is shown.

Figure 6

Residual distribution for Case 9 in the volume in which the grid search for the best source location is conducted. One vertical section sliced at 100 m south of the center of the crater is shown. Horizontal extent of the slice is 1500 m in the east-west direction and 2500 m in the vertical direction. Two local minimum are seen at (-400, -100, 1500) and (-300, -100, 0). The horizontal axes show the distance from the center of the summit crater. The vertical axis shows elevation above sea level. The residual value increases from blue to red. The bar range on the right is from 100% to 160 % of the smallest residual.

Figure 7

Source time functions for Case 9 ('3SF + 3SF'). The '3SF' source located at (-300, -100, 0) is on the left and the '3SF' source fixed at (-200, -100, 2250) is on the right. Horizontal axes represent time and vertical axes represent amplitude. From the top to the bottom of each panel, east-west, north-south, and vertical components are shown.

Figure 8

Source-time histories of the 'Fz' component for the 5 explosions on 1, 23, 29 September, 10 October, and 14 November. Horizontal axes represent time and vertical axes represent amplitude. The five panels are vertically aligned so that initial downward phases coincide with each other. For all 5 cases, a positive signal corresponding to an

upward force follows the initial negative phase (thin line). Five to 6 seconds later, another downward phase (shaded area) appears for all five explosions.

Figure 9

Two models of the vertical distribution of the single-force components exerted on the volcanic conduit. Lengths of the arrows indicate the strength of the drag force. (a) The magma column has no bottom. In this case, the downward single force is not concentrated. (b) The magma column has a constriction. Any structure that can effectively support the vertical component of the drag force in order for the magma column and the rest of the earth to exchange total linear momentum would work as conduit discontinuity. A constriction or a sharp bend in the conduit is a good candidate for such discontinuity.

Figure 10

Comparison between source locations (right) obtained by waveform analyses and the hypocenter distribution of volcanic earthquakes (left) determined by the double-difference method. Source locations for 10 cases are shown with error bars superimposed on the E-W section. Error bars correspond to 10 % increment above the minimum error. Cases 8, 9, and 10 are the two-point-source cases, and for these cases, one of the point sources is fixed at the source location for Case 4 (closed square). The other source is searched. For Case 9, two locations (closed triangles) give almost the same residual errors and AIC values.

Figure 11

Source-time functions obtained for Case 7 (top) and Case 10 (bottom). Horizontal axes are time and vertical axes are amplitude. For Case 7, the locations of point sources of six moment-tensor components and three single-force components are the same, while they are located at different positions for Case 10. Source locations are shown at the top of each panel.

Table captions

Table 1

Residual errors and corresponding Akaike's Information Criterion (AIC) for the 7 source mechanisms considered in the waveform analyses assuming a single point source. 'Fz' represents the vertical single force components. '6Mom' refers to the 6 moment tensor components. 'SF' and 'ISO' refer to the single force and isotropic components, respectively. Case 7 shows the best solution for single point source.

Table 2

Residual errors and AIC for the 3 cases assuming two point sources. One of the two point sources with three single forces is spatially fixed. The locations of the other point forces with various source mechanisms are grid-searched. The same abbreviations as used in Table 1 are used for the source mechanisms. The locations of unfixed sources are also shown. Case 10 shows the best solution of all 10 cases.

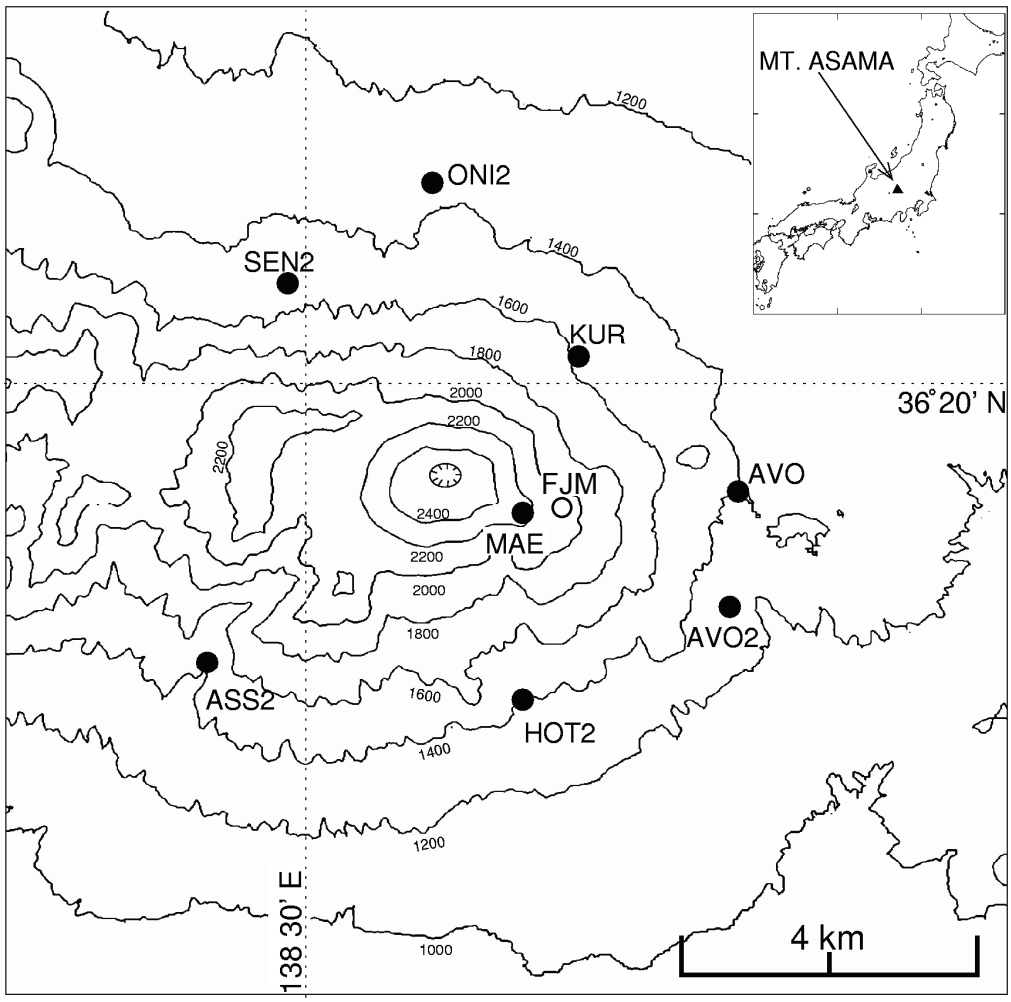
MT. ASAMA
ONI2
SEN2
KUR
FJM
O
MAE
AVO
AVO2
ASS2
HOT2
36°20' N
138°30' E
4 km
1200
1400
1600
1800
2000
2200
2400
1000

Figure 1

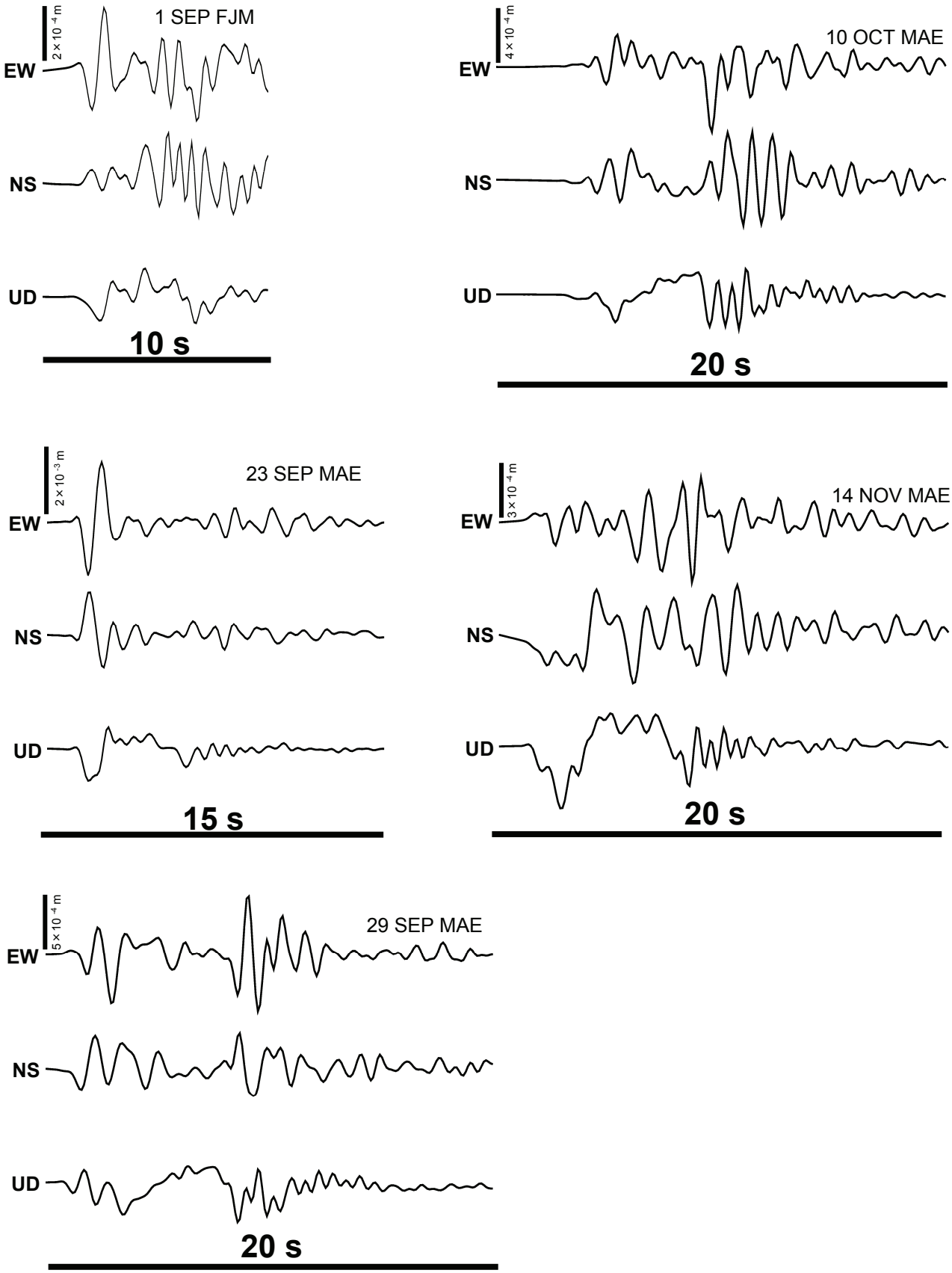
1 SEP FJM
2 × 10 -4 m
EW
NS
UD
10 s
10 OCT MAE
4 × 10 -4 m
EW
NS
UD
20 s
23 SEP MAE
2 × 10 -3 m
EW
NS
UD
15 s
14 NOV MAE
3 × 10 -4 m
EW
NS
UD
20 s
29 SEP MAE
5 × 10 -4 m
EW
NS
UD
20 s

Figure 2

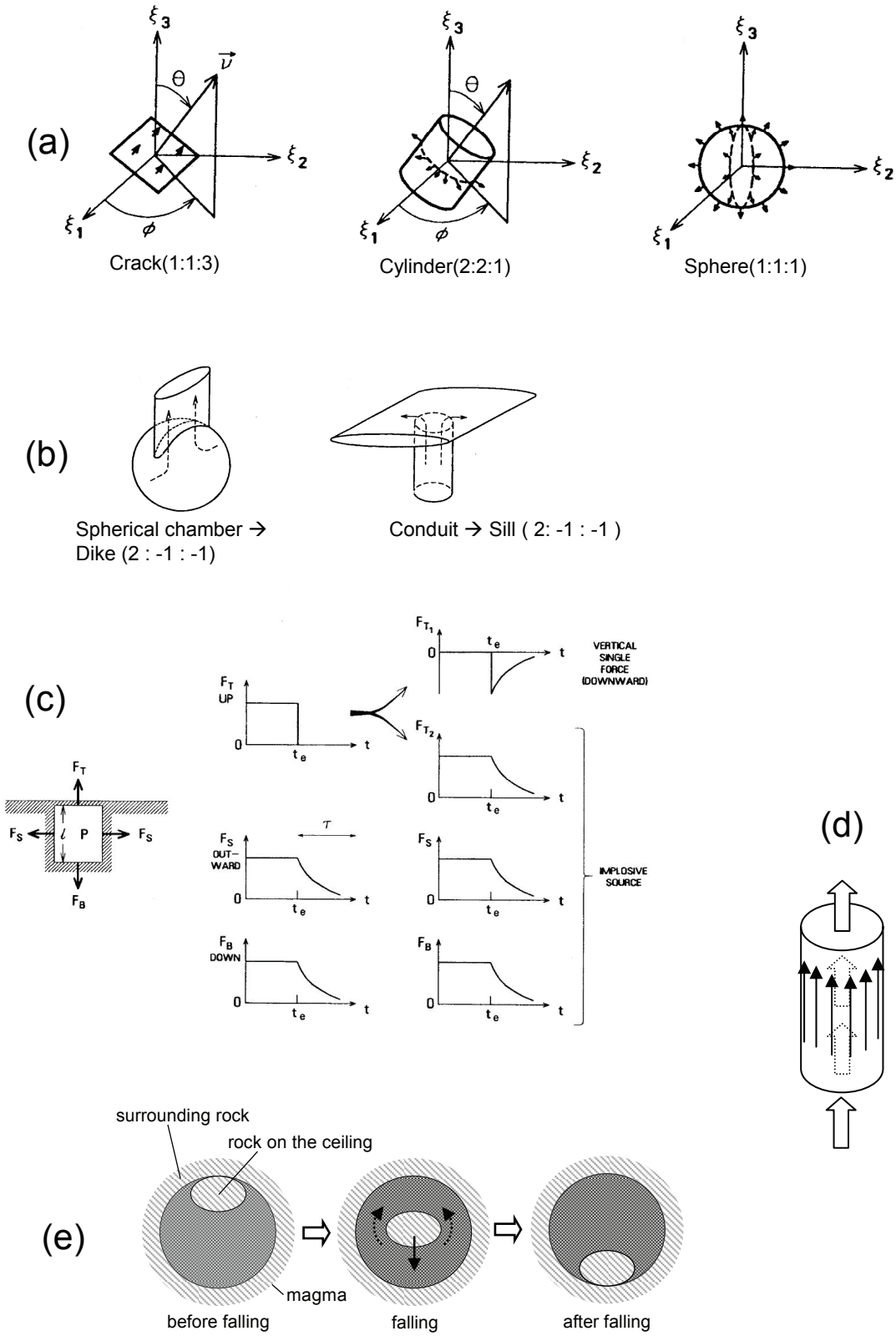
(a)
Crack(1:1:3)
Cylinder(2:2:1)
Sphere(1:1:1)
(b)
Spherical chamber → Dike (2 : -1 : -1)
Conduit → Sill (2: -1 : -1)
(c)
VERTICAL SINGLE FORCE (DOWNWARD)
IMPLOSIVE SOURCE
(d)
(e)
surrounding rock
rock on the ceiling
magma
before falling
falling
after falling

Figure 3

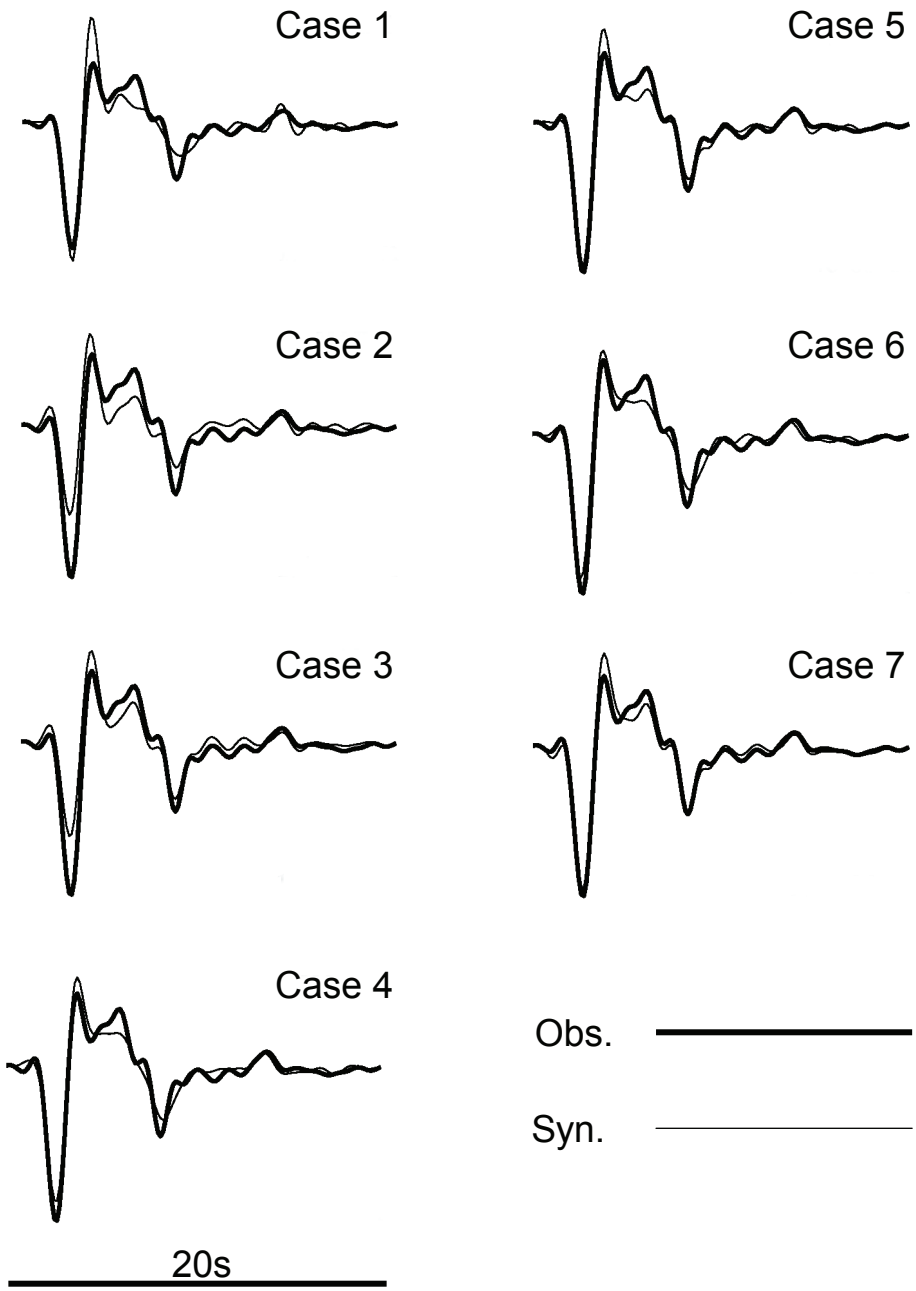

Figure 4

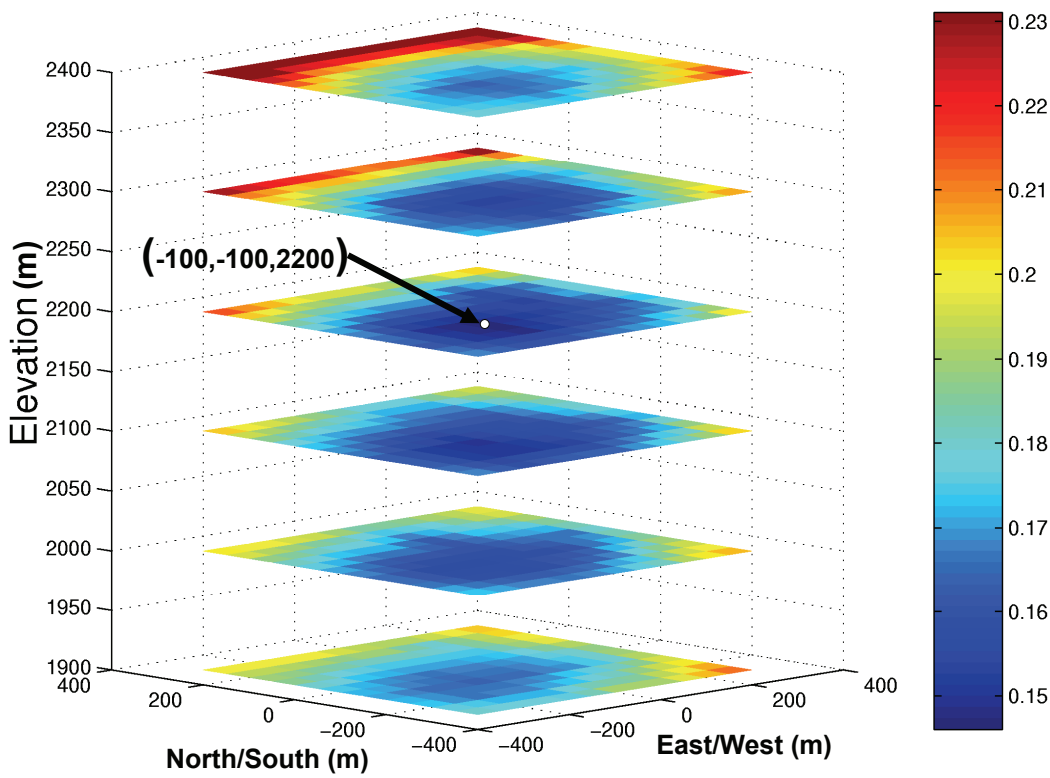
Elevation (m)
2400
2350
2300
2250
2200
2150
2100
2050
2000
1950
1900
(-100,-100,2200)
North/South (m)
400
200
0
−200
−400
East/West (m)
−400
−200
0
200
400
0.23
0.22
0.21
0.2
0.19
0.18
0.17
0.16
0.15

Figure 5

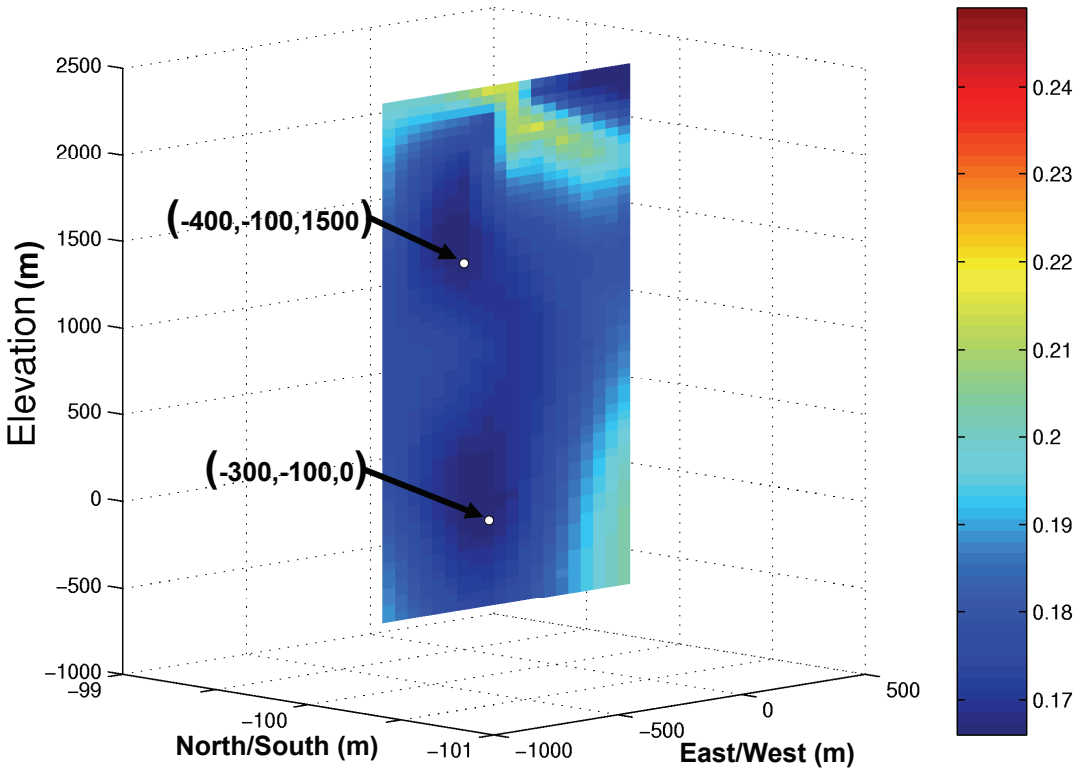
Elevation (m)
2500
2000
1500
1000
500
0
−500
−1000
(-400,-100,1500)
(-300,-100,0)
−99
−100
−101
North/South (m)
−1000
−500
0
500
East/West (m)
0.24
0.23
0.22
0.21
0.2
0.19
0.18
0.17

Figure 6

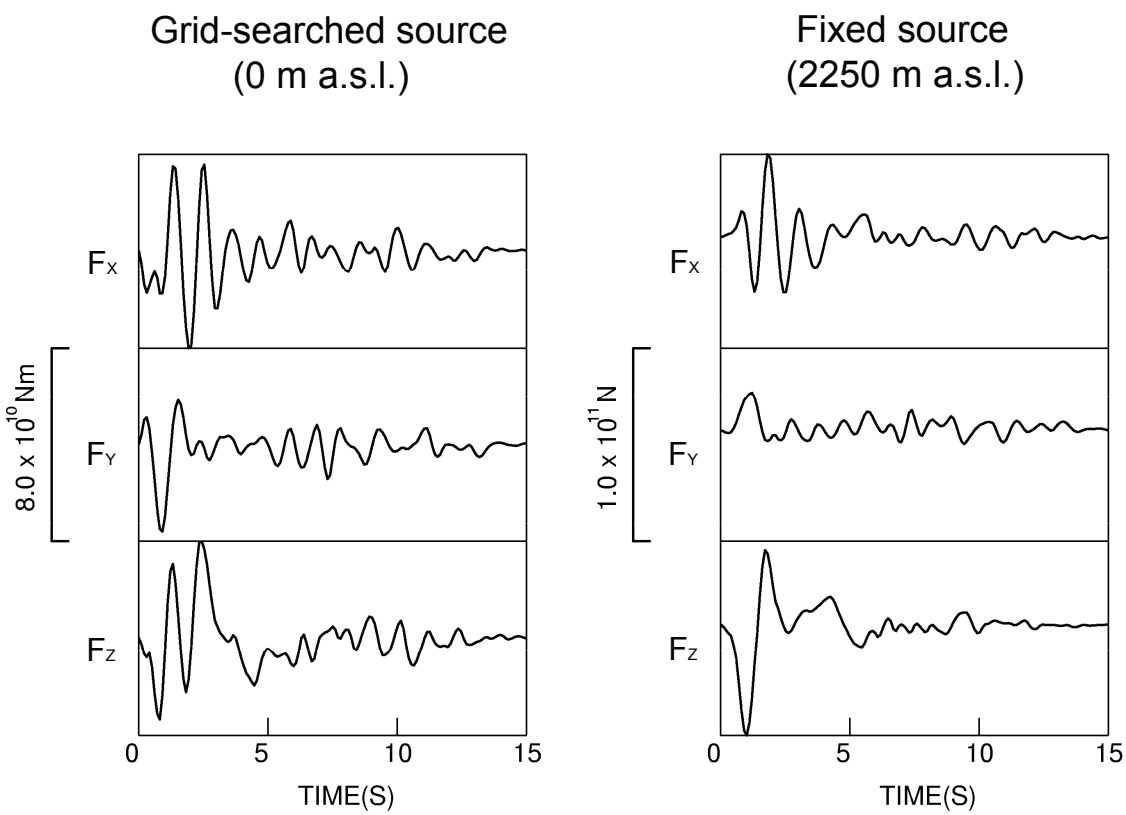
Grid-searched source
(0 m a.s.l.)
Fixed source
(2250 m a.s.l.)
Fx
FY
FZ
8.0 x 10^10 Nm
1.0 x 10^11 N
0
5
10
15
TIME(S)

Figure 7

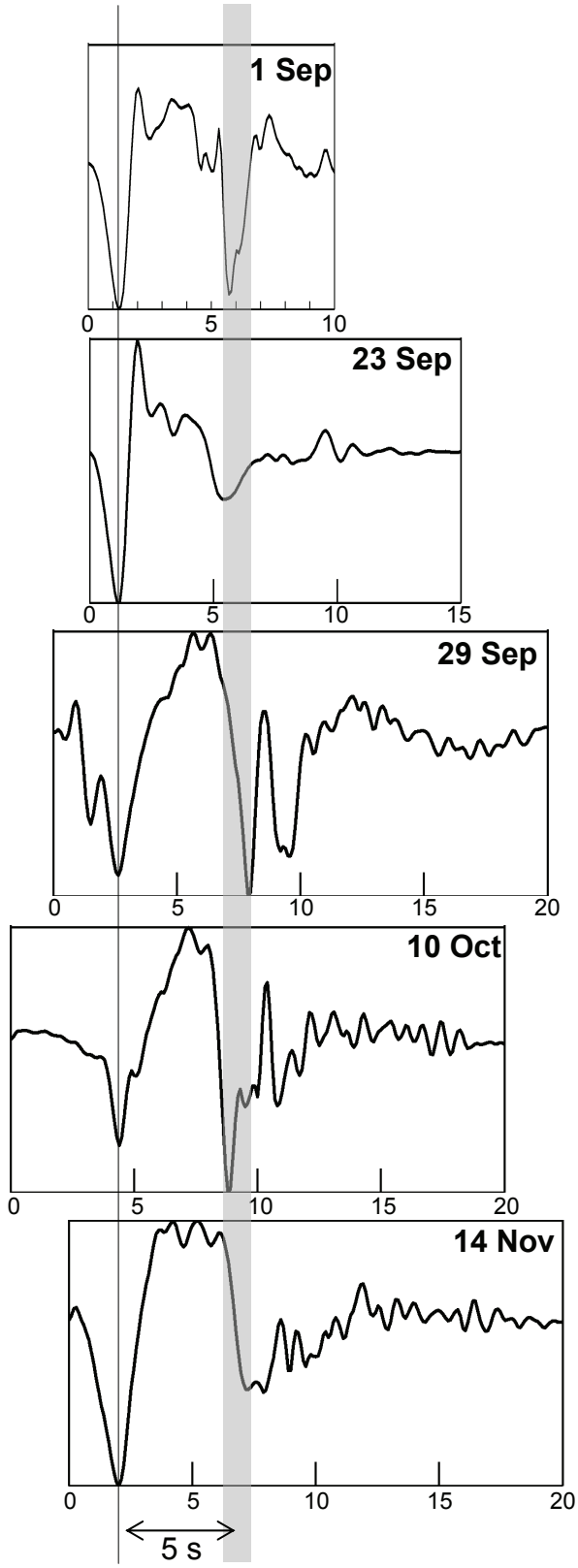
1 Sep
0
5
10
23 Sep
0
5
10
15
29 Sep
0
5
10
15
20
10 Oct
0
5
10
15
20
14 Nov
0
5
10
15
20
5 s

Figure 8

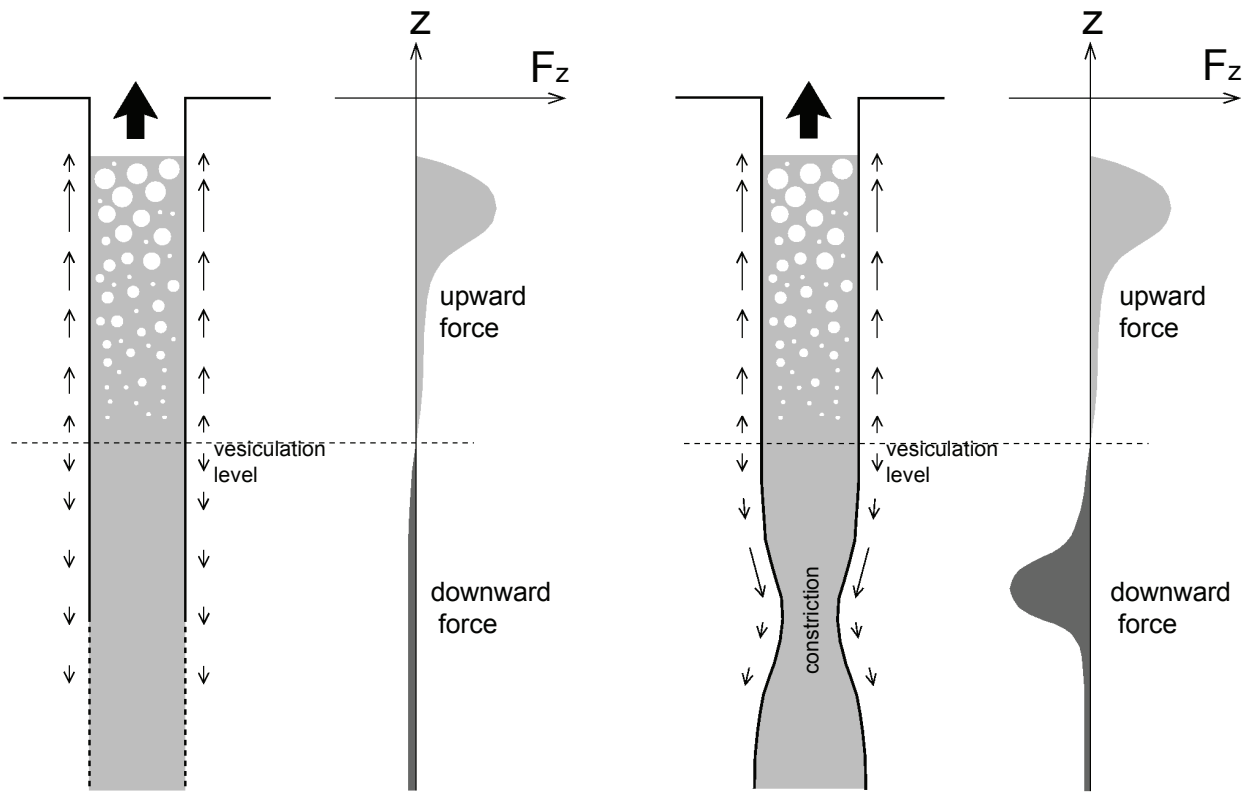

(a) Without constriction

(b) With constriction

Figure 9

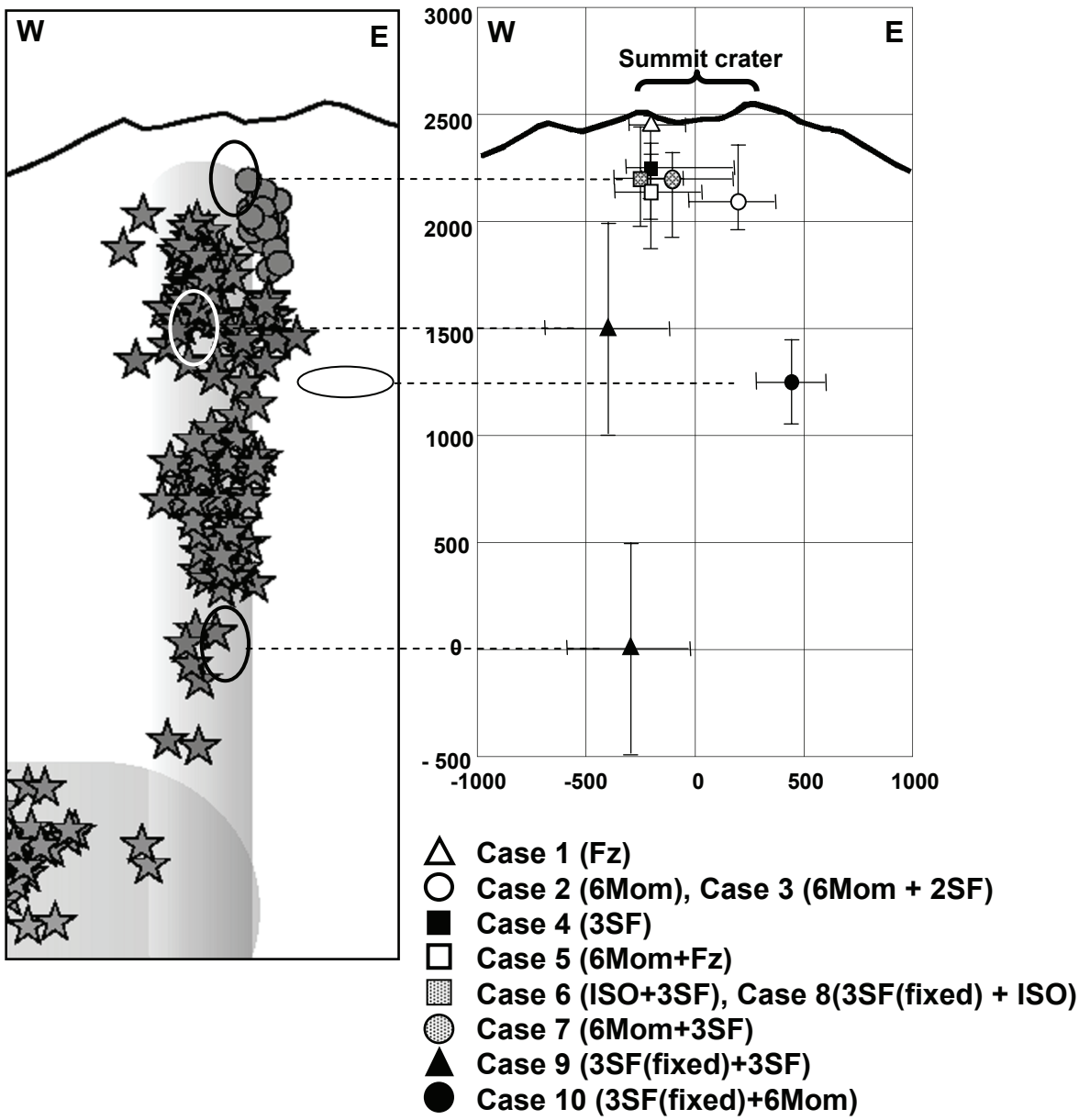
W
E
W
E
Summit crater
3000
2500
2000
1500
1000
500
0
- 500
-1000
-500
0
500
1000
Case 1 (Fz)
Case 2 (6Mom), Case 3 (6Mom + 2SF)
Case 4 (3SF)
Case 5 (6Mom+Fz)
Case 6 (ISO+3SF), Case 8(3SF(fixed) + ISO)
Case 7 (6Mom+3SF)
Case 9 (3SF(fixed)+3SF)
Case 10 (3SF(fixed)+6Mom)

Figure 10

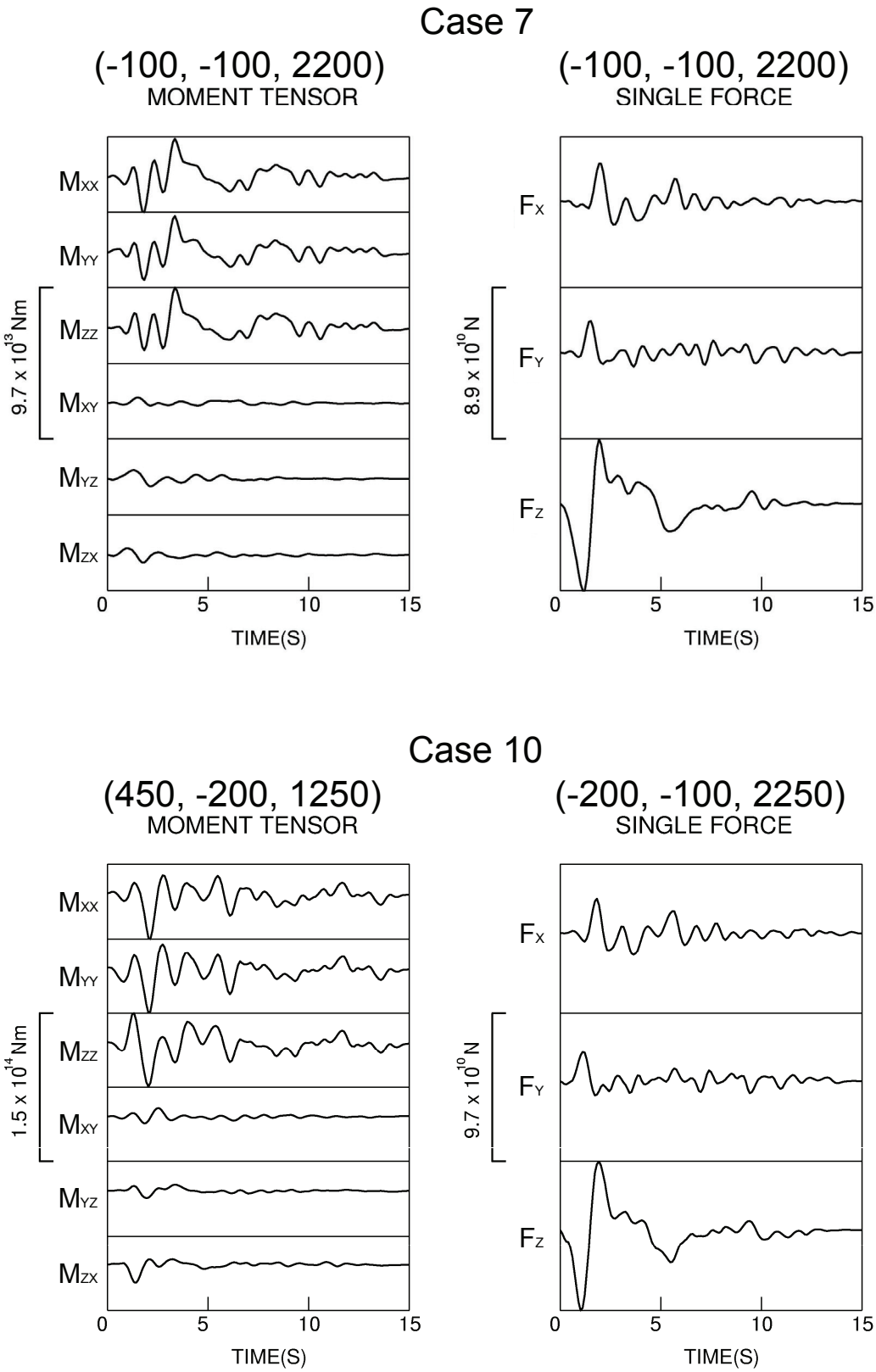
Case 7
(-100, -100, 2200)
MOMENT TENSOR
(-100, -100, 2200)
SINGLE FORCE
Mxx
Myy
Mzz
Mxy
Myz
Mzx
9.7 x 10^13 Nm
Fx
Fy
Fz
8.9 x 10^10 N
0
5
10
15
TIME(S)
Case 10
(450, -200, 1250)
MOMENT TENSOR
(-200, -100, 2250)
SINGLE FORCE
1.5 x 10^14 Nm
9.7 x 10^10 N

Figure 11

Mechanisms (**Mom**: moment, **SF**:single force **ISO**: isotropic volume source)	**Error**	**AIC**
Case 1: 'Fz'	0.512	-4671
Case 2: '6 Mom'	0.317	-7382
Case 3: '6 Mom + 2SF(Horizontal)'	0.238	-9138
Case 4: '3 SF'	0.260	-9244
Case 5: '6 Mom + Fz'	0.202	-10466
Case 6: 'ISO + 3 SF'	0.205	-10810
Case 7: '6 Mom + 3 SF'	0.146	-12504

Table 1: Residual errors and corresponding Akaike's Information Criterion (AIC) for the 7 source mechanisms considered in the waveform analyses assuming a single point source. 'Fz' represents the vertical single force components. '6Mom' refers to the 6 moment tensor components. 'SF' and 'ISO' refer to the single force and isotropic components, respectively. Case 7 shows the best solution for single point source.

Mechanisms (**Mom**: moment, **SF**:single force **ISO**: isotropic volume source)	**Error**	**AIC**	**Location of the unfixed source (ISO, 3SF, 6Mom)**
Case 8: '3 SF (fixed) + ISO'	0.205	-10810	ISO : same as the fixed one
Case 9: '3 SF (fixed) + 3 SF'	0.166	-12041	3SF : deep and slightly west
Case 10: '3 SF (fixed) + 6 Mom'	0.119	-14000	6Mom : deep and east

Table 2 : Residual errors and AIC for the 3 cases assuming two point sources. One of the two point sources with three single forces is spatially fixed. The locations of the other point forces with various source mechanisms are grid-searched. The same abbreviations as used in Table 1 are used for the source mechanisms. The locations of unfixed sources are also shown. Case 10 shows the best solution of all 10 cases.